Hindawi
International Journal of Energy Research
Volume 2023, Article ID 9919748, 14 pages
https://doi.org/10.1155/2023/9919748

Research Article

Exsolved Ru on $BaCe_xO_y$ Catalysts for Thermochemical Ammonia Synthesis

Arash Badakhsh,[1,2] **Hizkia Manuel Vieri**,[2,3] **Hyuntae Sohn**,[2,3] **Sung Pil Yoon**,[2] **and Sun Hee Choi**[2,3]

[1]*PNDC, University of Strathclyde, Glasgow, G68 0EF, UK*
[2]*Center for Hydrogen and Fuel Cell Research, Clean Technology Research Division, Korea Institute of Science and Technology (KIST), Seoul 02792, Republic of Korea*
[3]*Department of Energy and Environmental Engineering, KIST School, University of Science & Technology (UST), Seoul 02792, Republic of Korea*

Correspondence should be addressed to Sun Hee Choi; shchoi@kist.re.kr

Arash Badakhsh and Hizkia Manuel Vieri contributed equally to this work.

Received 6 January 2023; Revised 27 February 2023; Accepted 18 March 2023; Published 31 March 2023

Academic Editor: Pawan Kumar Kulriya

Ammonia (NH_3) is a carbon-free and hydrogen-rich (17.8 wt% H_2) chemical that has the potential to revolutionize the energy sector. Compared with hydrogen (H_2), NH_3 can be easily liquefied, stored, and transported globally. However, the conventional thermocatalytic process to synthesize NH_3 accounts for 2% of global energy consumption and 1.2% of CO_2 emissions annually. To make the process further efficient, new catalysts must be developed to allow for NH_3 synthesis in milder conditions with high thermal stability. To this end, we have developed ruthenium (Ru) supported on perovskite ($BaCe_xO_y$) via a ball-milling-assisted exsolution method that allows for a more tunable morphology. Reactivity is compared with the catalyst prepared via the conventional impregnation technique. The as-synthesized catalysts are characterized by XRD, H_2-TPR, TEM, XPS, and APT. The NH_3 synthesis is carried out in a packed-bed tube reactor thermochemically. Using N_2 instead of Ar as the carrier gas during exsolution can favour reactivity by increasing active sites and perhaps improving metal-support interaction. The impregnated sample shows higher reactivity than the exsolved catalyst; however, the long-term durability is slightly better using the exsolved catalyst. Finally, APT results interestingly show that the exsolved catalyst is more resistant to hydride formation and hydrogen poisoning, which is one of the main deactivation mechanisms for such metallic catalysts.

1. Introduction

Ammonia (NH_3) is among the most promising alternative fuels to replace carbon-based energy carriers [1]. Not only does it have a high volumetric energy density (15.6 MJ/L; 70% more than liquid hydrogen (H_2) [1]), but also it is a crucial ingredient in many industries, such as agriculture (in fertilizers) and pharmaceuticals (*e.g.*, in antimicrobial agents). Its mild liquefaction conditions (-30°C at 1 atm or 25°C at 10 atm) also make this hydrogen-rich molecule (17.8 wt% H_2) favourable as a chemical hydrogen (H_2) carrier [2, 3]. To unlock the full potential of this influential material, however, further research is necessary to mitigate the energy required for its production (*i.e.*, ~2% of global energy consumption [1]) and the resultant emissions (*i.e.*, ~1.2% of anthropogenic CO_2 emissions [4]).

Conventionally, NH_3 is synthesized via the Haber-Bosch process, which requires high temperature and pressure catalytic reactors [4]. Even though NH_3 synthesis is thermodynamically exothermic (see Equation (1)), the catalysts and

reactants need to be activated to dissociate the nitrogen (N_2) and hydrogen (H_2) bonds. Catalysts for this process are usually made of cost-effective iron (Fe) supported on ceramics. However, noble and more costly metals such as ruthenium (Ru) are more active. Leveraging metals with higher reactivity can effectively reduce the reaction condition and, in turn, mitigate the energy consumption and emissions from burning fuels.

$$3H_2 + N_2 \longrightarrow 2NH_3, \quad \Delta H^{\circ}_{27^{\circ}C} = -46.35\,\text{kJ/mol}. \tag{1}$$

Furthermore, the deactivation of catalysts in NH_3 synthesis is mainly via three main mechanisms: (i) sulfur poisoning and/or coking when H_2 is supplied via methane reforming; (ii) H_2 poisoning and metal hydride formation; and (iii) sintering of catalyst nanoparticles at high temperature [5]. The recent advances in H_2 production by water electrolysis eliminate the problem (i). However, the regeneration of catalysts after sintering remains challenging without rigorous chemical treatment [6]. Exsolution of metals from oxide support offers a solution for recyclable and functional catalysts [7]. In this method, the metal is first embedded within the bulk crystal lattice of the oxide support—usually the B site in perovskites—and it is drawn to the surface by gradual reduction of the compound. Oxygen vacancies created by the reducing agent result in the nucleation of the metal on the surface of the support. This technique allows for the regeneration of the deactivated catalyst via consecutive calcination and reduction cycles. Another advantage of exsolution over impregnation is the synthesis of well-exposed metallic nanocatalysts, which enhances the mass transfer of the reactants to the catalyst on the surface with a strong metal-support interface [8].

Despite the advantages of exsolution, literature to date lacks the application of this technique in thermochemical NH_3 synthesis catalyst development and/or thorough investigation of pros and cons of exsolved catalysts. For instance, Kosaka et al. [9] synthesized and analyzed exsolved Ru on $BaCe_{0.9}Y_{0.1}O_3$ support for electrochemical NH_3 synthesis with the maximum rate of 3.3 mol/s/$mg_{exsolved\text{-}Ru}$ at 500°C. Moreover, numerous studies have been conducted on exsolution of Ni catalysts [10, 11], but literature on exsolved Ru is rather a new research topic. Some of the recent studies on the exsolution of Ru include $Sm_2Ru_xCe_{2-x}O_7$ for methane dry reforming [12], $Ln_2Ru_{0.2}Ce_{1.8}O_7$ (Ln = Sm, Nd, La) in propene hydrogenation [13], and $La_{2-x}NiRuO_{6-\delta}$ ($x = 0.1$ and 0.15) as electrocatalysts [14]. Evidently, there is a lack of studies on exsolved Ru specifically for NH_3 synthesis as one of the most vital industrial reactions. Additionally, studies have shown that $BaCeO_3$ (BCO) is a promising support for Ru for NH_3 applications. This is speculated to be due to the combination of Ce^{3+}/Ce^{4+} redox ability—which increases the electron density of Ru—and strong basic sites [15, 16]. In another attempt, Kitano et al. [17] synthesized Ru on BCO oxynitride-hydride support via the solid-state reaction for low-temperature NH_3 synthesis.

To see the effect of fabrication and Ru exsolution conditions on the thermochemical NH_3 synthesis, we were prompted to study this promising catalytic compound (Ru-doped BCO) for such a highly demanded reaction. The long-term stability of samples prepared via exsolution or conventional wet impregnation was also compared. We aimed to leverage exsolution for the facile synthesis of regenerable and functional catalysts for NH_3 applications. Herein, we propose a simplified protocol to synthesize exsolved Ru on perovskite supports. The as-synthesized catalysts were characterized via transmission electron microscopy (TEM), X-ray diffractometry (XRD), H_2 temperature-programmed reduction (H_2-TPR), X-ray photoelectron spectroscopy (XPS), and atom probe tomography (APT). The performance of the exsolved Ru catalysts in NH_3 synthesis and decomposition was investigated, and methods for increasing the reactivity of exsolved Ru catalysts are identified and discussed.

2. Experimental

2.1. Materials. Barium carbonate ($BaCO_3$, 99.99%, Sigma-Aldrich), cerium(IV) oxide (CeO_2, 99.9%, Sigma-Aldrich), and triruthenium dodecacarbonyl ($Ru_3(CO)_{12}$, 99%, Sigma-Aldrich) were used as Ba, Ce, and Ru precursors, respectively. Tetrahydrofuran (THF, anhydrous, 99.99%, Sigma-Aldrich) was used as the solvent for the impregnated samples. All the reagents were used without further purification, unless stated otherwise.

2.2. Catalyst Fabrication. Exsolved Ru catalysts were supported on barium cerium oxide ($BaCe_xRu_{1-x}O_3$, BCRO). The following describes the protocol for facile synthesis of exsolved Ru catalysts: (i) the precursor powders were ball milled (3 h at 300 rpm or 6 h at 600 rpm) and mixed at stoichiometric ratios, where Ru loading was fixed at 5 wt%; (ii) the pulverized compound (yellow) was then placed inside an alumina (Al_2O_3) boat and calcined in a muffle furnace for 5 h at 900°C (5°C/min) in static air; (iii) calcined powder (dark brown) was then reduced at 900°C (2.5°C/min) for X = 1, 3, 6, 9, 12, and 15 h under flowing 10% H_2/Ar or 10% H_2/N_2 (100 NmL/min) to obtain the exsolved Ru on BCO.

Impregnated samples were prepared via a stepwise wet impregnation method: (i) BCO support was prepared via the aforementioned ball-milling method; (ii) $Ru_3(CO)_{12}$ was dissolved in THF at room temperature (RT), and the calcined BCO was also dispersed in THF at RT; (iii) the prepared Ru solution was then added to the BCO suspension and magnetically stirred for 12 h at RT; (iv) the remaining THF was evaporated at RT under a fume hood, and the collected powder was then dried at 80°C overnight in a convection oven; (v) the impregnated catalyst was then calcined at 500°C (5°C/min) for 5 h in flowing Ar; and (vi) lastly, the catalysts were reduced at 450°C (5°C/min) for 1 h in flowing 10% H_2/N_2.

2.3. Catalyst Characterizations. Transmission electron microscopy (TEM) image and energy-dispersive spectroscopy (EDS) mapping were analyzed by a TEM-Talos, which was operated at an accelerating voltage of 200 kV and a

magnification of 80,000,000x. The particle size distribution of Ru nanoparticles was determined using the ImageJ software.

Atom probe tomography (APT) needle-shaped specimens were prepared using a dual-beam scanning electron microscope/focused ion beam (Helios NanoLab 650, FEI) following the site-specific "lift-out" method. The specimens were measured in a local electrode atom probe (LEAP 4000 X Si, Cameca) with pulsed laser mode with a repetition rate of 100 kHz and pulse fraction of 50% for exsolved catalyst 100% for the impregnated catalyst. The detection rate was two ions per 1000 pulses (0.2%) on average. The base temperature of the specimen was 50 K. The acquired data of samples were reconstructed using Imago Visualization & Analysis System software (IVAS 3.8.4, AMETEK, USA).

Wide-angle X-ray diffraction (XRD) patterns were recorded in the 2θ range of 10-90° using the SmartLab SE instrument (Rigaku, Tokyo, Japan) operated at 30 kV and 20 mA, with Cu Kα radiation ($\lambda = 1.54$ Å) used as the X-ray source.

Temperature-programmed reduction (H_2-TPR) was carried out in a BELCAT-M chemisorption analyzer (MicrotracBEL Corp.). The sample was loaded in a customized double-layer wall quartz reactor, where the two ends were connected to a Swagelok fitting to allow reactant gases to pass through the catalyst bed. The stepwise process is described below:

(i) Around 0.07 g of sample was first pretreated at 300°C for 1 h under pure Ar (99.999%) gas to remove any impurity or water from the surface

(ii) The temperature was then decreased to 30°C and maintained until a stable TCD baseline was obtained

(iii) After switching the gas to 10% H_2/Ar, the temperature was increased to 900°C at a ramp rate of 5°C/min and was maintained for 15 min

Ru metal dispersion was also determined by CO chemisorption using the BELCAT-M chemisorption analyzer (MicrotracBEL Corp.). The stepwise process is described below:

(i) First and similarly to H_2-TPR measurement, 0.07 of the reduced catalyst was placed in the reactor

(ii) The temperature was then increased to 150°C at 10°C/min under flowing 5% H_2/Ar. The temperature was maintained for 30 min

(iii) Then, the sample was cooled down naturally to 50°C, followed by pulsed CO injection for the measurement

(iv) CO pulses were repeated for at least 10 times until the peak retained its area and height for three consecutive peaks

(v) The active Ru dispersion was then calculated by using the sum of adsorbed CO assuming stoichiometry factor of one (Ru : CO = 1 : 1)

The specific surface areas of the catalysts were measured by the Brunauer-Emmett-Teller (BET) method. The stepwise process is described below:

(i) The samples were first pretreated at 70°C for 2 h under a vacuum

(ii) The temperature was then increased to 200°C, and the samples were further degassed for around 12 h until the pressure was maintained below 60-70 mTorr

(iii) After degassing, the temperature was decreased to room temperature (RT) and the sample tube was transferred to the analysis port which flowed with N_2. The amount of adsorbed N_2 was measured with the Micromeritics ASAP 2420 instrument. The N_2 adsorption isotherms of the samples were measured at the liquid nitrogen temperature

(iv) The Barrett-Joyner-Halenda (BJH) pore size distribution was determined from the desorption branch of the isotherm

The electronic state of Ru, Ba, Ce, and O in prepared catalysts was analyzed by the XPS instrument (XPS, K-Alpha+, Thermo Scientific) equipped with monochromatic Al Kα radiation. The binding energy was corrected according to carbon 1s binding energy (284.8 eV). XPS fitting was done using XPSPEAK41 software.

2.4. Ammonia (NH_3) Synthesis Test. The reactivity of the catalysts in NH_3 synthesis was evaluated in stainless steel (3/8″) tubular reactor with varying temperatures (300, 325, 350, 375, and 400°C) and relative pressure (0, 10, 20, and 30 bars). The reactor setup piping and instrumentation diagram (P&ID) is shown in Figure 1. 0.1 g of catalyst powder was sandwiched between glass wool beds and Al_2O_3 beads (1~2 mm in diameter). The NH_3 synthesis rate was collected by titration method, where the effluent gas was absorbed in 0.1 M aqueous sulphuric acid (H_2SO_4, 95-98%, Sigma-Aldrich), and the solution's electrical conductivity was recorded via a conductivity meter (Orion Star A212, Thermo Scientific).

3. Results and Discussion

3.1. Selection of Reduction Conditions. Figure 2(a) shows the X-ray diffractograms of the BCO support, Imp, and Ex powders. For all samples, peaks were detected at similar Bragg angles. Li et al. [15] also reported the XRD results obtained for Ru on BCO catalysts in addition to the reference peaks for BCO (PDF#22-0074). The obtained diffractograms can be further compared against the XRD patterns provided by the Materials Project [18] as a reliable database. For a scan range of 20–80°, the corresponding XRD peaks for cubic perovskite BCO are located at $2\theta = 28.2$, 40.3, 49.9, 58.3, 66.0, and 73.3°. Additionally, a lattice parameter calculation was carried out to compare our data with the reference. A negligible error of 1.4%, 1.3%, and 1.4% was found for BCO, Imp, and Ex, respectively, when compared to the reference *a* constant value of 4.47 Å.

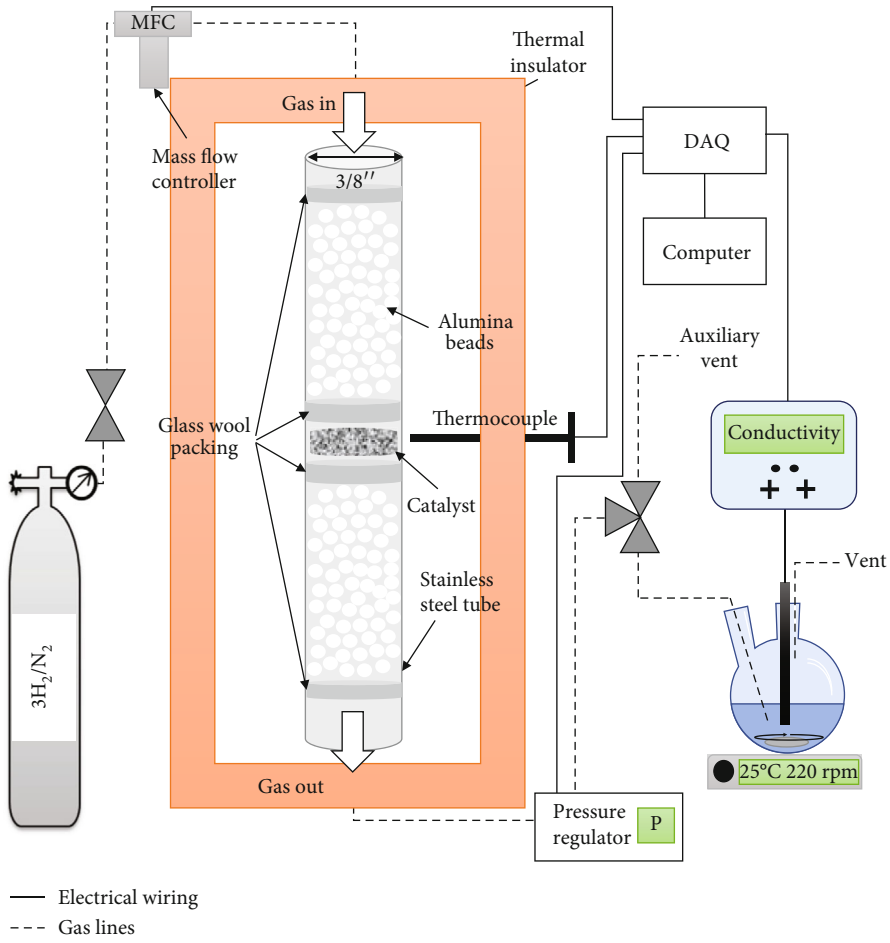

Figure 1: NH_3 synthesis and detection setup.

The H_2-TPR thermograms, shown in Figure 2(b), were obtained for the support and Ru/support catalysts to delineate the proper reduction temperature and exsolution temperature for impregnated and exsolved samples. Unfortunately, the available reports on this subject are lacking comprehensive testing and data availability. For example, the latest relevant study published in December 2022 fails to provide the H_2-TPR results [19]. Therefore, we have resorted to deductive reasoning by the process of elimination when comparing our H_2-TPR results and the possible answers from the available literature. The following is the summary of our findings.

Broadening of the peaks for the BCO support and impregnated sample is suspected to be the result of interaction of different species, which was also reported by Morlanés et al. [20] associated with the systems containing Ba and Ce. They also conclude that Ba may facilitate the reduction of Ce. Here, BCO support shows a constant reduction starting at 236.5°C with a sharp peak at 829.6°C, which can be attributed to the start of the reduction of surface oxygen species followed by reduction of the oxygen species in the bulk of the material. Therefore, the right temperature for exsolution of Ru out of the bulk of the BCO was selected at 900°C. This can also be seen with the emergence of a peak at 777.2°C for the exsolved sample, which is absent in the impregnated case.

For the impregnated sample, the main reduction peaks are observed at 106. 8°C and 466.1°C. Hence, the reduction for the impregnated sample was opted to be at 450°C for 1 h. The peaks observed at 80–120°C and 450–500°C are attributed to the reduction of Ru^{4+} to metallic Ru and the support surface oxygen species, respectively [21, 22]. Some references imply that the peak at 450–500°C could be also attributed to the reduction of bulk Ru [23, 24]. The latter might be the correct assumption as there is no peak detected at this range for the bare BCO powder. More recent studies divide the H_2-TPR peaks into two parts, the higher temperature region which correspond to RuO_x reduction (α-H_2) and higher temperature region which corresponds to RuO_x interaction with support (ß-H_2) [25–27]. Hence, the peak observed at 466.1 could be associated with the interaction of RuO_x and BaO and/or CeO_2 species. However, it is most likely to be RuO_x and BaO when comparing with the trends obtained in our work on impregnated Ru on $La_2Ce_2O_7$ catalysts currently under revision. Another explanation could be the effect of Ru precursor, which is in our case triruthenium dodecacarbonyl. Li et al. [15] in their study on the impregnated Ru on BCO support for thermochemical ammonia synthesis reported a lower temperature peak detected at 300–400°C range. They used ruthenium acetylacetonate as the Ru precursor. Therefore, we deduce that the

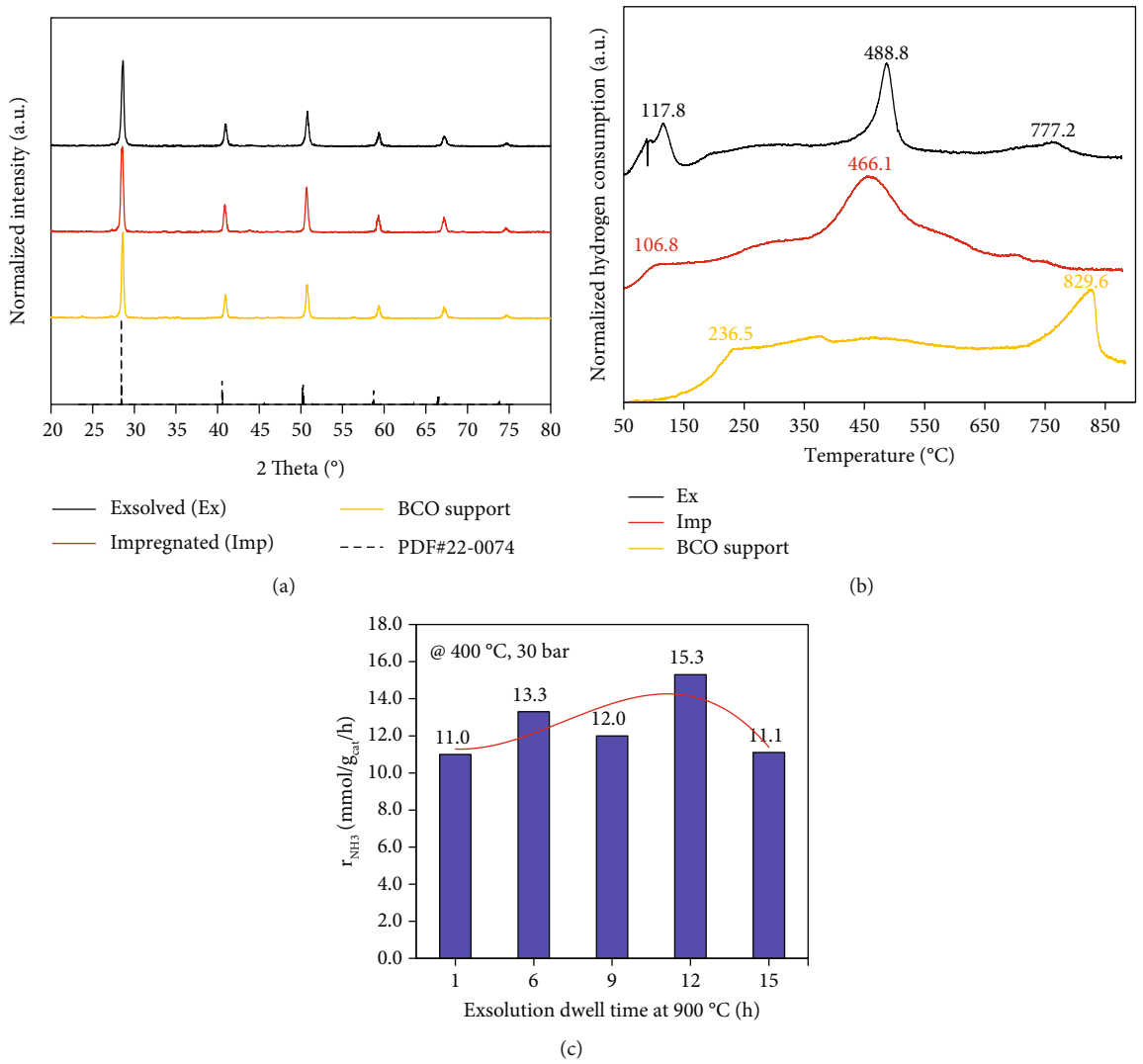

FIGURE 2: (a) XRD patterns of Ex, Imp, BCO, and reference BCO. (b) TPR profiles of Ex, Imp, and BCO. (c) Effect of exsolution time of Ex on its NH_3 synthesis activity.

chemistry of the Ru precursor can also influence the interaction of RuO_x with other species.

Finally, regardless of the explanation, a lower Ru reduction peak detected observed at 80–120°C can indicate a stronger metal-support interaction [28]. Therefore, H_2-TPR thermograms obtained here show better interaction in the exsolved sample.

To select the appropriate exsolution time, reactivity of catalysts reduced at 900°C with various dwell times was obtained at the reaction temperature of 400°C and pressure of 30 bars. The results are shown in Figure 2(c). The screening results indicate that the NH_3 production rate increases up to 12 h and then decreases back to almost the same value as 1 h of exsolution after 15 h. This could be attributed to the lower degree of exsolved Ru after 9 h from the bulk to the surface where it is available for reacting with the gaseous reactants (*i.e.*, mass transfer limitation). The decreasing trend after 12 h could be caused by larger Ru nanoparticles resulting from sintering after long residence time at such a high temperature. Hence, 12 h was selected as the optimum exsolution time at 900°C. TEM images and EDS mapping of the catalysts before and after exsolution for 12 h are shown in Figure 3 (see also Figure S1). Figure 3 provides morphological evidence of successful exsolution of Ru from BCO support.

3.2. Ball-Milling Effect. In powder engineering, ball milling is one of the readily available techniques for pulverizing and mixing purposes. Previous studies have shown that ball-milling conditions can dramatically affect the size of nanoparticles and their dispersion within the matrix in composite compounds [29, 30]. Hence, in this study, the reactivity of catalysts prepared by low-intensity (LIBM: 3 h at 300 rpm) and high-intensity (HIBM: 6 h at 600 rpm) planetary ball milling was tested, and the results are shown in Figures 4(a) and 4(a′). As seen here, the NH_3 synthesis rate is much higher (up to 4.8 times at 400°C and 30 bars) in the case of high-intensity preparation. As evidenced by Figures 4(b) and 4(b′), this higher reactivity is attributed to the better dispersion of Ru nanoparticles when ball milled with higher intensity. As a result, other catalysts were prepared by HIBM for further analyses.

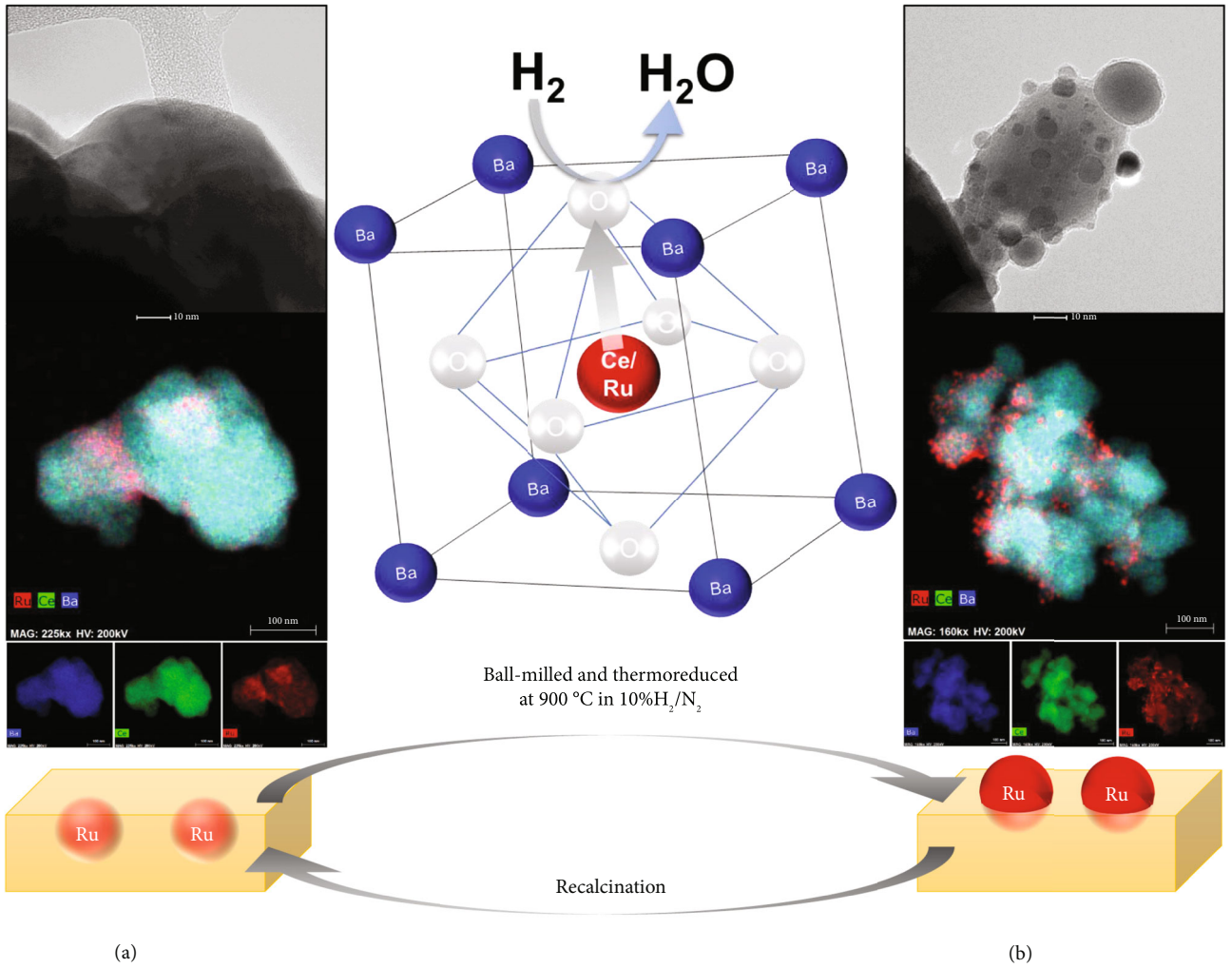

Figure 3: Bright-field TEM images and EDS mapping of (a) calcined and (b) 12 h exsolved catalysts. The intermediate schematics illustrate the exsolution mechanism.

3.3. NH_3 Synthesis Rate. In their study, Ye et al. [31] showed that thermal treatment of Ce-based support under N_2 environment leads to the formation of CeN with nitrogen vacancies that are active for N_2 reduction. In another study, they also confirmed that nitrogen vacancies in lanthanide supports can lead to highly functional catalysts for NH_3 synthesis with a reactivity comparable to Ru-based catalysts [32]. Therefore, we have been prompted to also evaluate the effect of carrier gas during exsolution on the formation of N_2 activation sites.

Dissociation of nitrogen atoms and breaking the stable and strong triple bonds of N_2 are the rate-determining steps when considering the kinetics of NH_3 synthesis. Aside from the reduction temperature, the reducing gas can affect the properties of NH_3 synthesis catalyst. Instead of using pure H_2 or Ar carrier for H_2, the use of N_2 instead of Ar can create surface nitrogen vacancies which can accelerate N_2 activation [32] and facilitate N_2 adsorption and step-by-step hydrogenation of N_2 to $^*HNNH$, $*NH{\cdot}NH_3$, and $^*NH_2{\cdot}NH_4$ [33]. Based on NH_3 synthesis rate, shown in Figure 5, the 10% H_2/N_2-reduced catalysts showed a higher NH_3 synthesis rate than 10% H_2/Ar-reduced catalysts. This is true for both Imp and Ex samples; however, Ex catalysts exhibit more sensitivity to the reducing environment—for Imp, the reaction rate at 400°C and 30 bars increased 15%, whereas Ex showed a 100% increase. This could be rooted in the nature of exsolution that essentially occurs under a reducing agent.

These results show that using N_2 as the carrier gas during exsolution can result in chemical changes in the catalyst. This could also be due to formation of nitride sites on the support which increases the metal-support interaction. Figure S2 shows an increase in the reduction temperature of support surface species when using N_2 as carrier, which was also observed by Hu et al. [34] after doping the support of their Ru-based catalyst with nitrogen. This may confirm our theory on the advantage of incorporation of nitrogen into the support chemistry.

As shown in Table 1, replacing Ar with N_2 as the reducing carrier gas for the exsolved catalyst increases the Ru dispersion significantly, *i.e.*, by about 20 times. This could further explain the advantages of nitrogen vacancies within the support that promote the active sites on the metallic nanoparticles by perhaps electron donation properties. In terms of surface area, the Ar-treated sample

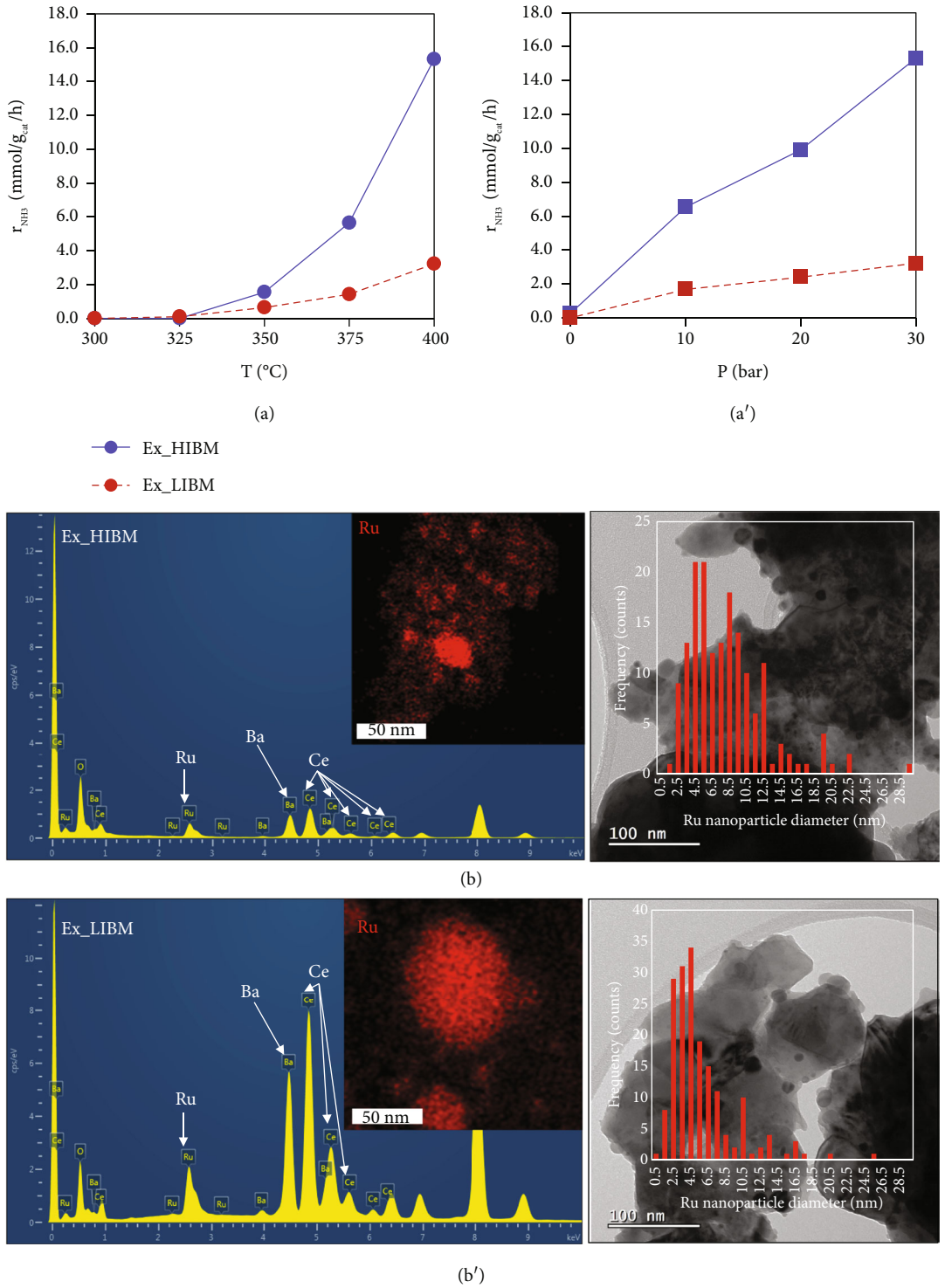

Figure 4: NH_3 synthesis rate of exsolved catalyst ball milled at 600 rpm for 6 h and 300 rpm for 3 h with respect to (a) reaction temperature change at 30 bars and (a′) reaction pressure change at 400°C. EDS maps and high-angle annular dark-field (HAADF) images of catalyst ball milled at (b) 600 rpm for 6 h and (b′) 300 rpm for 3 h.

shows almost as twice as the N_2-treated catalyst. This could be attributed to two main factors: (i) measurement of surface area by N_2 adsorption and less interaction with N_2-activated catalysts; (ii) treatment with Ar, which is denser than N_2, may lead to the increase in pore size and dispersion [35, 36].

3.4. Long-Term Reactivity. Thermal durability of the Ex and Imp catalysts was investigated. As shown in Figure 6 (see also Table S1), Ex shows a noticeably higher reactivity during the first 20 h of reaction before decreasing in the similar rate with the Ex catalyst. The results indicate that the exsolution of Ru from BCO support led to a slightly more stable

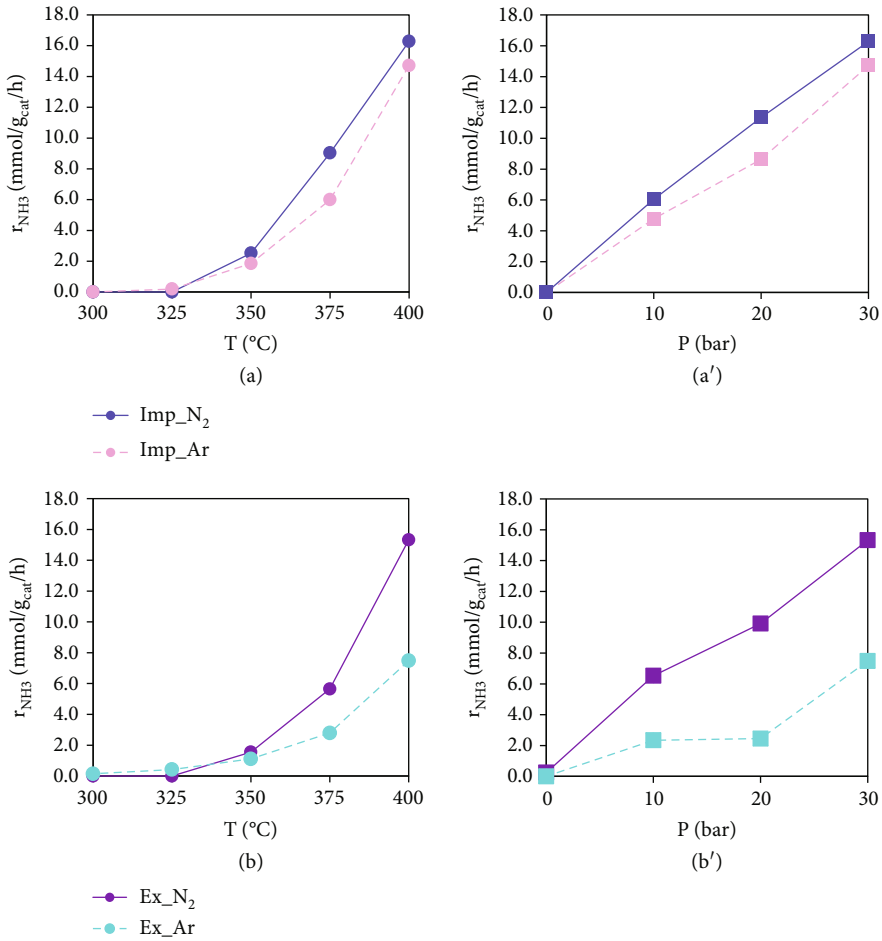

Figure 5: NH_3 synthesis rate of (a) impregnated and (b) exsolved catalyst that reduced under different gases with dependence on temperature at 30 bars and pressure at 400°C.

Table 1: Calculated Ru metal dispersion and specific surface area of impregnated and exsolved catalyst reduced at different conditions.

Catalyst	Metal dispersion (%)	Specific surface area (m^2/g)	Average pore size[a] (Å)	Pore volume[b] (cm^3/g)
Imp_N_2	4.9288	4.0900	119	0.0121
Ex_N_2	7.8028	3.1792	132	0.0105
Ex_Ar	0.3909	5.6776	245	0.0347

[a]Pore size was calculated based on adsorption average pore width (4 V/A by BET). [b]Pore volume was calculated by single-point N_2 adsorption.

catalyst than the one prepared by means of incipient wetness impregnation. Morphological evaluation of the TEM images before and after the long-term test also does not reveal a noticeable change in Ru nanoparticle size before and after the long-term test. However, the width of the particle size distribution of Ex is broader than that of Imp, and it shows a multimodal distribution curve. This implies that Ru was dispersed better when exsolved. This further confirms a better metal-support interaction in the exsolved sample, also deduced from H_2-TPR thermograms. We suspect that Ex samples may offer both better chemical stability and physical stability. Hence, further chemical examination of Ex and Imp was carried out using XPS and APT.

From Figure 7(a), it can be observed that after reaction (Ex_Spent_N_2 and Imp_Spent_N_2), the catalyst had the Ba 3d shifted to the left (high binding energy). If we compare the Ex_Fresh_N_2 and Imp_Fresh_N_2, we observe that the exsolved samples have a higher oxidation state. The peak position of Ce 3d is visualized in Figure 7(b). The Ce^{3+} concentration is related to the number of oxygen vacancies on the $BaCeO_3$ surface, which can be estimated from the area ratio of Ce^{3+} peaks to Ce^{4+} peaks [37]. To be more specific, the ratio of Ce^{3+}/Ce^{4+} (Figure 7(c)) is higher as well on the impregnated catalyst (Imp_Fresh_N_2) compared to the exsolved catalyst (Ex_Fresh_N_2).

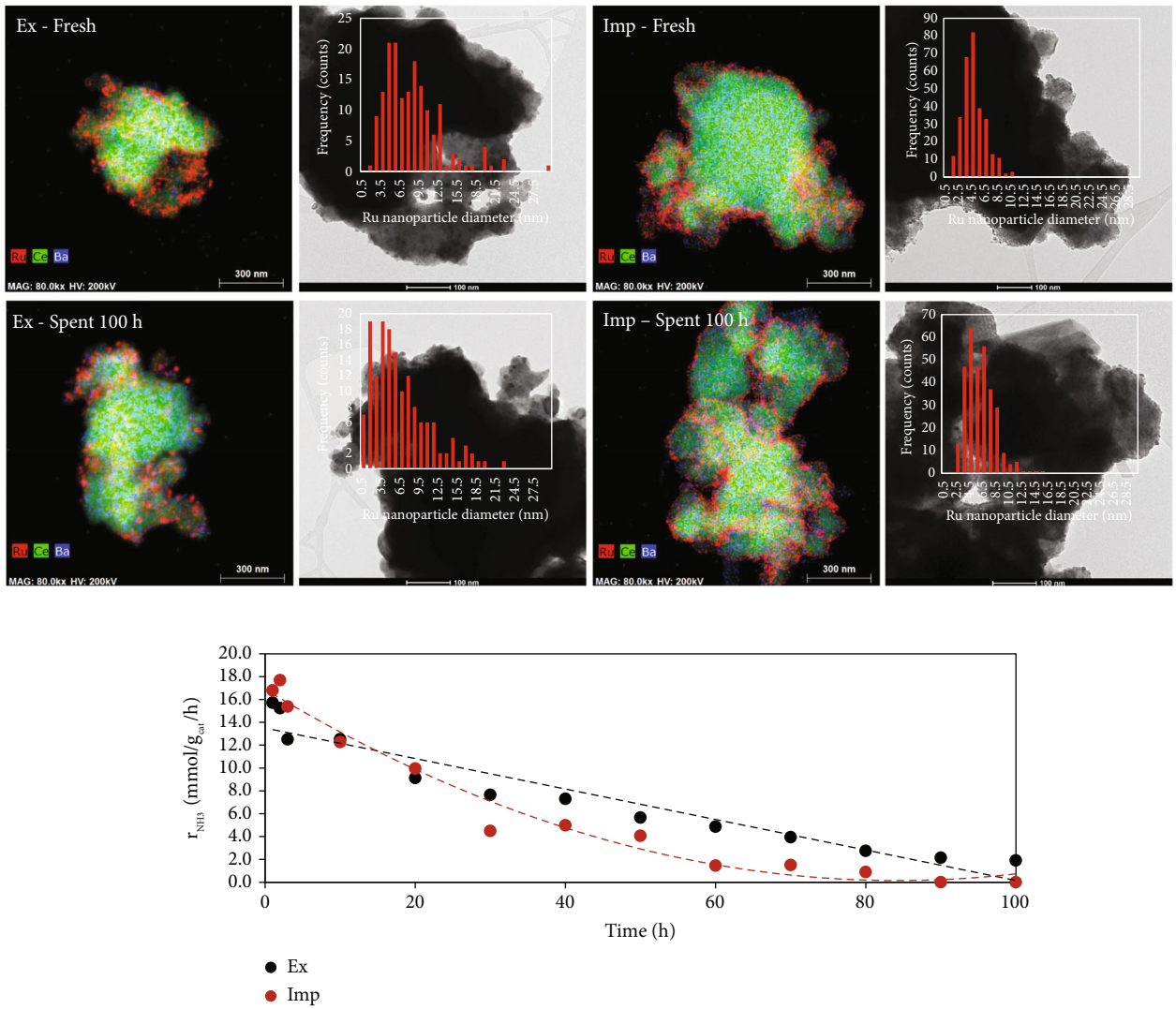

FIGURE 6: EDS mapping, high-angle annular dark-field (HAADF) images, and long-term NH_3 synthesis rate of exsolved and impregnated catalysts; the long-term tests were conducted at 400°C and 30 bars.

The Ru 3d spectra of the BCRO and BCOR catalyst are shown in Figure 7(d). The chemical state of Ru on the catalysts was investigated on the basis of the Ru $3d_{5/2}$ and Ru $3d_{3/2}$. However, the latter is not suitable for the analysis because there is strong overlapping with C 1s signal. Despite being low in intensity, the Ru $3d_{5/2}$ peaks recorded over Fresh_Imp_N_2 show two components at 280 and 281 eV which can be ascribed to Ru^0 and Ru^{4+}, respectively [38]. It is noted that the Ru $3d_{5/2}$ signal is absent in the cases of Ex_Fresh_Ar, Ex_Fresh_N_2, and Ex_Spent_N_2. That is possibly due to the nature of exsolved catalyst, where most of the Ru are incorporated into the lattice rather than staying on the surface. The area ratio of $Ru^0/(Ru^0 + Ru^{n+})$ is 0% and 35% for Ex_Fresh_N_2 and Imp_Fresh_N_2, respectively. The high percentage of Ru^0 in Fresh_Imp_N_2 indicates a high electron density of Ru species in that catalyst, which is beneficial for the dissociation of N_2 triple bonds. A high amount of Ru^0 also can indicate the performance of a catalyst. The impregnated catalyst, once again, showed more amount of Ru^0 compared to exsolved catalyst. When we see the Ru $3p_{5/2}$ spectra of those catalysts, the impregnated catalysts (Imp_Fresh_N_2) have a higher oxidation state compared with the exsolved catalyst (Ex_Fresh_N_2). Considering that the overlap between the C 1s and Ru 3d peaks makes the results dependent on the deconvolution, the Ru 3p profiles were also analyzed to provide additional evidence (Figure 7(e)).

The O 1s profiles of Figure 7(f) are fitted with two peaks. The one at 531.4 eV is ascribed to surface-adsorbed oxygen species (O_{ads}), while that at 529.3 eV to lattice oxygen (O_{latt}) of RuO_2 and/or $BaCeO_3$ [39]. For Imp_Fresh_N_2 (82%), the amount of surface-adsorbed oxygen is higher than that of the Ex_Fresh_N_2 (3%), and the $O_{ads}/(O_{ads} + O_{latt})$ ratios of the catalysts follow the order of Ex_Spent_N_2 (100%), Imp_Fresh_N_2 (82%), Imp_Spent_N_2 (55%), Ex_Fresh_Ar (48%), and Ex_Fresh_N_2 (3%).

Finally, we can summarize our findings as the following:

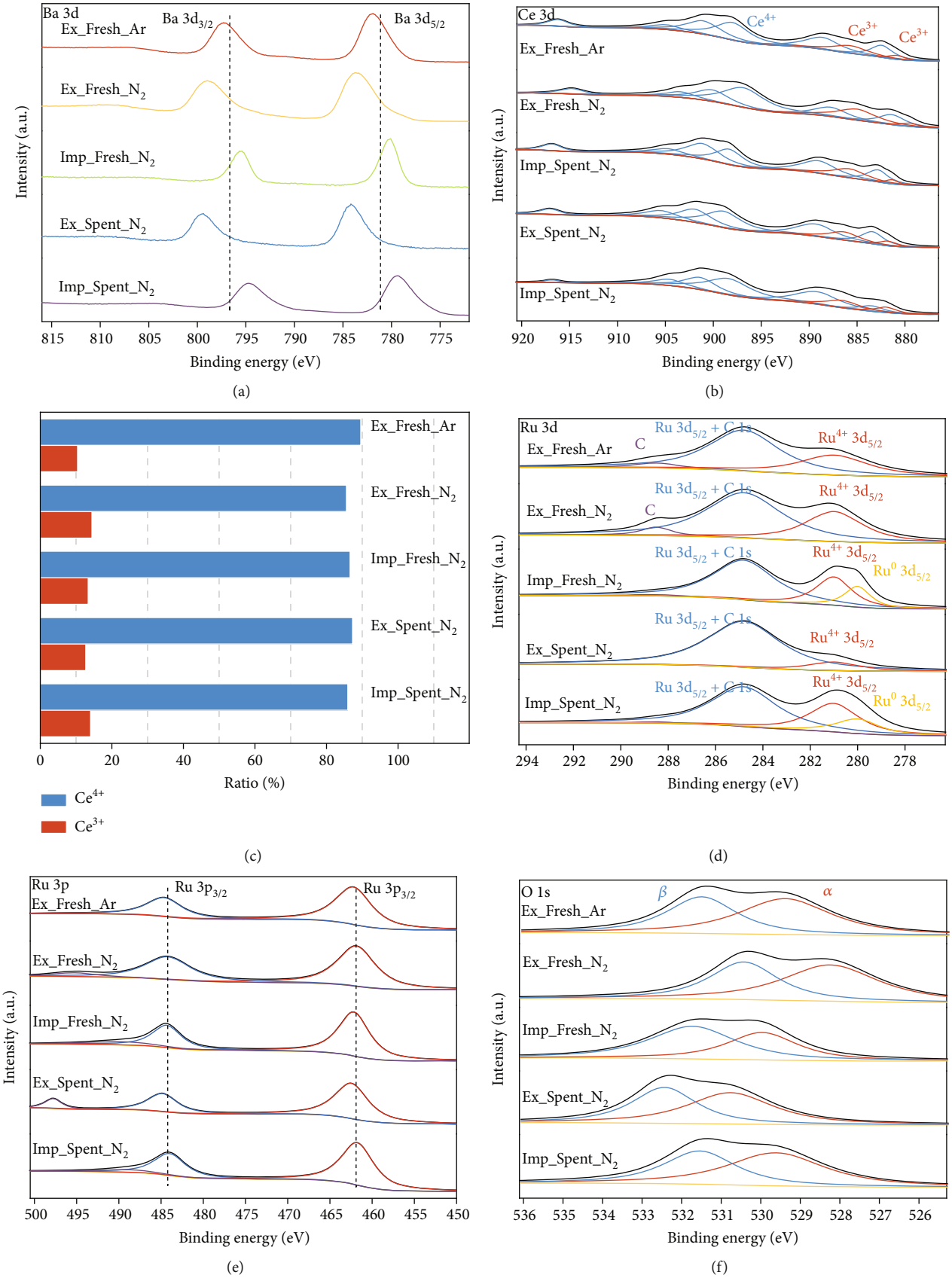

Figure 7: (a) Ba 3d, (b) Ce 3d, (c) Ce^{3+}/Ce^{4+} composition, (d) Ru 3d, (e) Ru 3p, and (f) O 1s XPS spectra of exsolved and impregnated catalysts.

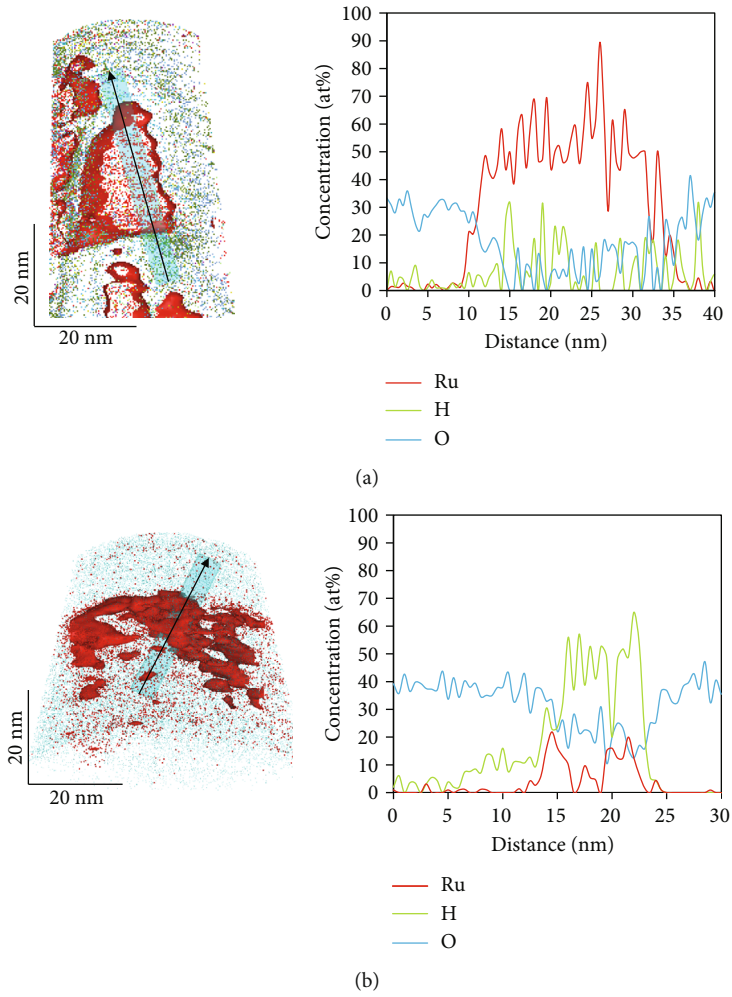

Figure 8: Atom probe tomography (APT) of spent (a) exsolved and (b) impregnated catalysts.

(i) Exsolved catalysts have less surface Ru since they are dissolved more in the lattice

(ii) Comparing the Ce peaks, more oxygen vacancies were observed for Imp

(iii) Studying the oxygen dispersion, more oxygen vacancies were observed in the sample exsolved in N_2. However, after 100 h of reaction, all the lattice oxygen species have migrated to the surface of the exsolved sample. We assume this means that exsolution was not complete and continued while conducting the NH_3 reaction. On the other hand, surface oxygen species of Imp was reduced by 28% after NH_3 synthesis reaction which could be attributed to the reduction of surface oxygen during the reaction. Overall, a dramatic increase in surface oxygen species after reaction for Ex and the inverse trend in Imp indicate that formation of water, rather than NH_3, is more dominant for Ex compared with Imp

Atom probe tomography (APT) was used to provide a 3d map of elemental composition of the catalysts after 100 h of reaction at 400°C and 30 bars. The scale measured in APT is very small, typically ~100-500 nm, and it provides high-resolution tomography with high chemical sensitivity of a limited region. APT maps are reconstructed based on the computations and the measurement of evaporation rate of different ions present in the sample. APT was carried out to determine whether the Ru is present in the oxide, hydride, or metallic state after 100 h of reaction. Figure 8 (see also Figure S3) shows atomic maps of the entire APT-measured volume and the concentration of Ru, H, and O across the scanned area. From this image, it can be clearly seen that the exsolved catalyst shows a high concentration of metallic Ru—favourable to catalytic reaction—rather than the high concentration of Ru hydride and oxide apparent in the impregnated sample. This supports the higher durability of the exsolved catalyst against chemical deactivation, also evidenced by the results of long-term reactivity test. Moreover, APT results show that Ru particle size is more dispersed in the exsolved sample than Imp. Kim et al. [19] also reported larger particles in Ex than Imp, which again corroborates with our APT findings.

3.5. Catalyst Regeneration. One advantage of exsolved catalysts is that they may enable regeneration of the catalyst deactivated by poisoning and/or sintering. By principle, the

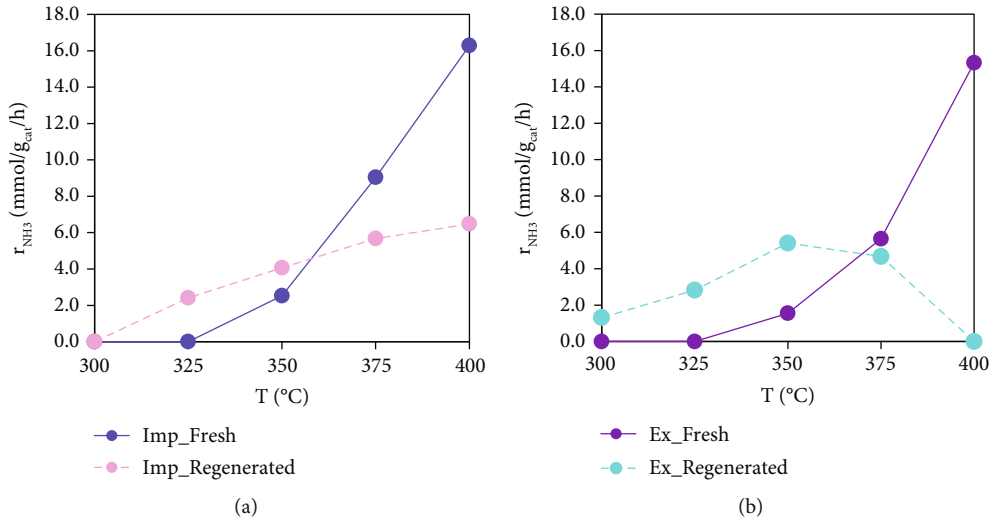

Figure 9: NH_3 synthesis rate of (a) impregnated and (b) exsolved catalyst before and after regeneration with dependence on temperature at 30 bars.

Ru nanoparticles exsolved on the surface can be integrated with the lattice and return to the bulk by calcination and nucleate back to the surface with consecutive exsolution in a reducing environment. Therefore, to evaluate this capability and compare it with the Imp sample, catalyst regeneration was conducted by recalcination and rereduction of catalysts using their corresponding condition.

Figure 9 shows the reactivity trends after regeneration. Essentially, it can be seen that the reaction equilibrium is shifted to lower temperatures for both Imp and Ex catalysts after regeneration, albeit the maximum reactivity obtained for the catalysts is reduced dramatically after regeneration. Even though it was expected to regenerate better, the exsolved catalyst only maintained 65% of its initial reaction rate while the impregnated catalyst can maintain 73% of its initial reaction rate (see Equation (2)). However, regenerated Ex exhibits higher reactivity at a milder temperature (350°C at 30 bars) which is the highest compared with the NH_3 synthesis rate of fresh and regenerated Imp and fresh Ex. Altogether, this implies a higher reactivity of active sites, perhaps B5 sites [40], but lower number of active sites in the regenerated samples.

$$*\text{regeneration rate} : \frac{\overline{r_{NH_3}}\,[\text{regenerated}]}{\overline{r_{NH_3}}\,[\text{fresh}]}. \quad (2)$$

4. Conclusions

This paper has studied the exsolution of Ru from $BaCe_xO_y$ support and the reactivity of the as-developed catalyst in thermochemical NH_3 synthesis. This was attempted with a thorough comparison of performance and characteristics with samples prepared via the conventional impregnation catalyst synthesis method. Morphology, reactivity, long-term stability, chemical state, and regeneration of catalysts prepared via exsolution and impregnation are presented. XRD and TEM results confirm the successful exsolution of Ru from $BaCe_xO_y$ lattice of the powder prepared via ball milling and reacted in solid state. High-intensity ball milling is shown to improve Ru dispersion. Using N_2 as the carrier gas during exsolution in a reducing environment can improve the metal-support interaction leading to better catalyst reactivity compared with when Ar is used as the carrier. NH_3 synthesis rate of 15.3 mmol/$g_{catalyst}$·h at 3 MPa (N_2 : H_2 = 1 : 3) and 400°C was obtained for the N_2/H_2-redced sample which was more than two times higher than the synthesis rate of the catalyst exsolved in Ar/H_2. The results of XPS analysis suggest that the partial substitution of Ce by Ru for the synthesis of $BaCe_{1-x}RuO_3$ facilitates strong synergy between Ru and Ce species. The consequence is more $Ru^{\delta+}$ clusters and surface Ce^{3+} species in the exsolved sample, which are beneficial for N_2 adsorption and activation. The findings may foster further research for the design of efficient and stable catalysts for NH_3 synthesis under mild temperature and pressure. The long-term reactivity of the exsolved sample reveals a higher stability which warrants further investigation on the support-metal interaction on exsolved catalysts. Overall, our findings suggest that despite the slightly higher mass activity of impregnated catalyst, H_2-TPR, long-term durability analysis, APT, and regeneration evaluation of Ex suggest that exsolved catalysts are more resistant to hydrogen poisoning and it can shift the equilibrium to milder temperatures after regeneration.

Data Availability

The data used to support the findings of this study are available from the corresponding author upon request.

Additional Points

Highlights. (i) Exsolution of Ru via ball-mill-assisted solid-state reaction was proven versatile. (ii) Impregnated Ru on BCO showed similar reactivity with exsolved catalyst. (iii) Using N_2 as the carrier gas during exsolution can increase the active sites. (iv) Chemical durability of exsolved catalyst was better than impregnated.

Conflicts of Interest

The authors of this manuscript declare that there are no competing interests.

Authors' Contributions

Arash Badakhsh and Hizkia Manuel Vieri contributed equally to this work and are co-first authors.

Acknowledgments

This work was supported by the National Research Foundation of Korea (NRF), funded by the Korean Government (Ministry of ICT) (Grant No. 2021R1A2C2008662).

Supplementary Materials

Figure S1: bright-field TEM images of the exsolved catalyst with different magnifications; the inset on the right is the fast Fourier transform (FFT) image corresponding to the red outline. Figure S2: TPR thermograms of calcined samples obtained under flowing 10% H_2/Ar and 10% H_2/N_2. Table S1: XPS peak position and peak area of each catalyst. Figure S3: APT mapping of exsolved and impregnated catalysts. *(Supplementary Materials)*

References

[1] A. Valera-Medina, H. Xiao, M. Owen-Jones, W. I. F. David, and P. J. Bowen, "Ammonia for power," *Progress in Energy and Combustion Science*, vol. 69, pp. 63–102, 2018.

[2] A. Badakhsh, Y. Kwak, Y.-J. Lee et al., "A compact catalytic foam reactor for decomposition of ammonia by the Joule-heating mechanism," *Chemical Engineering Journal*, vol. 426, article 130802, 2021.

[3] A. Badakhsh, J. Cha, Y. Park et al., "Autothermal recirculating reactor (ARR) with Cu-BN composite as a stable reactor material for sustainable hydrogen release from ammonia," *Journal of Power Sources*, vol. 506, article 230081, 2021.

[4] C. Smith, A. K. Hill, and L. Torrente-Murciano, "Current and future role of Haber–Bosch ammonia in a carbon-free energy landscape," *Energy & Environmental Science*, vol. 13, no. 2, pp. 331–344, 2020.

[5] P. Nielsen, "Deactivation of synthesis catalyst," in *Catalytic Ammonia Synthesis*, pp. 285–301, Springer, 1991.

[6] J. Du, J. Gao, F. Gu et al., "A strategy to regenerate coked and sintered Ni/Al_2O_3 catalyst for methanation reaction," *International Journal of Hydrogen Energy*, vol. 43, no. 45, pp. 20661–20670, 2018.

[7] O. Kwon, S. Joo, S. Choi, S. Sengodan, and G. Kim, "Review on exsolution and its driving forces in perovskites," *Journal of Physics: Energy*, vol. 2, article 032001, 2020.

[8] D. Neagu, T.-S. Oh, D. N. Miller et al., "Nano-socketed nickel particles with enhanced coking resistance grown *in situ* by redox exsolution," *Nature Communications*, vol. 6, no. 1, p. 8120, 2015.

[9] F. Kosaka, T. Nakamura, and J. Otomo, "Electrochemical ammonia synthesis using mixed protonic-electronic conducting cathodes with exsolved Ru-nanoparticles in proton conducting electrolysis cells," *Journal of the Electrochemical Society*, vol. 164, no. 13, pp. F1323–F1330, 2017.

[10] A. L. Larralde, L. Troncoso, C. Alvarez-Galvan, V. Cascos, M. T. Fernandez-Díaz, and J. A. Alonso, "Defective $Sr_{0.9}Mo_{0.9}O_{3-\delta}$ perovskites with exsolved Ni nanoparticles as high-performance composite anodes for solid-oxide fuel cells," *New Journal of Chemistry*, vol. 45, no. 27, pp. 12041–12049, 2021.

[11] P. B. Managutti, S. Tymen, X. Liu et al., "Exsolution of Ni nanoparticles from A-site-deficient layered double perovskites for dry reforming of methane and as an anode material for a solid oxide fuel cell," *ACS Applied Materials & Interfaces*, vol. 13, no. 30, pp. 35719–35728, 2021.

[12] M. A. Naeem, P. M. Abdala, A. Armutlulu, S. M. Kim, A. Fedorov, and C. R. Müller, "Exsolution of metallic Ru nanoparticles from defective, fluorite-type solid solutions $Sm_2Ru_xCe_{2-x}O_7$ To impart stability on dry reforming catalysts," *ACS Catalysis*, vol. 10, no. 3, pp. 1923–1937, 2020.

[13] M. A. Naeem, D. B. Burueva, P. M. Abdala et al., "Deciphering the nature of Ru sites in reductively exsolved oxides with electronic and geometric metal–support interactions," *The Journal of Physical Chemistry C*, vol. 124, no. 46, pp. 25299–25307, 2020.

[14] J. Guo, R. Cai, E. Cali et al., "Low-temperature exsolution of Ni–Ru bimetallic nanoparticles from A-site deficient double perovskites," *Small*, vol. 18, article 2107020, 2022.

[15] W. Li, S. Wang, and J. Li, "Highly effective $_{Ru/BaCeO(3)}$ catalysts on supports with strong basic sites for ammonia synthesis," *Chemistry-An Asian Journal*, vol. 14, no. 16, pp. 2815–2821, 2019.

[16] X.-L. Yang, W.-Q. Zhang, C.-G. Xia, X.-M. Xiong, X.-Y. Mu, and B. Hu, "Low temperature ruthenium catalyst for ammonia synthesis supported on $BaCeO_3$ nanocrystals," *Catalysis Communications*, vol. 11, no. 10, pp. 867–870, 2010.

[17] M. Kitano, J. Kujirai, K. Ogasawara et al., "Low-temperature synthesis of perovskite oxynitride-hydrides as ammonia synthesis catalysts," *Journal of the American Chemical Society*, vol. 141, no. 51, pp. 20344–20353, 2019.

[18] A. Jain, S. P. Ong, G. Hautier et al., "Commentary: the materials project: a materials genome approach to accelerating materials innovation," *APL Materials*, vol. 1, no. 1, article 011002, 2013.

[19] H. Kim, A. Jan, D.-H. Kwon et al., "Exsolution of Ru nanoparticles on $BaCe_{0.9}Y_{0.1}O_{3-\delta}$ modifying geometry and electronic structure of Ru for ammonia synthesis reaction under mild conditions," *Small*, vol. 19, no. 6, p. 2205424, 2023.

[20] N. Morlanés, S. Sayas, G. Shterk et al., "Development of a Ba–CoCe catalyst for the efficient and stable decomposition of ammonia," *Catalysis Science & Technology*, vol. 11, no. 9, pp. 3014–3024, 2021.

[21] N. Jeon, S. Kim, A. Tayal et al., "Y-doped $BaCeO_3$ perovskite-supported Ru catalysts for CO_x-free hydrogen production from ammonia: effect of strong metal–support interactions," *ACS Sustainable Chemistry & Engineering*, vol. 10, no. 47, pp. 15564–15573, 2022.

[22] Y. Zhou, J. Wang, L. Liang et al., "Unraveling the size-dependent effect of Ru-based catalysts on ammonia synthesis at mild conditions," *Journal of Catalysis*, vol. 404, pp. 501–511, 2021.

[23] S. Cimino, L. Lisi, and S. Romanucci, "Catalysts for conversion of ethanol to butanol: effect of acid-base and redox properties," *Catalysis Today*, vol. 304, pp. 58–63, 2018.

[24] P. Liu, R. Niu, W. Li, S. Wang, and J. Li, "Morphology effect of ceria on the ammonia synthesis activity of Ru/CeO_2 catalysts," *Catalysis Letters*, vol. 149, no. 4, pp. 1007–1016, 2019.

[25] C. Li, F. Liu, Y. Shi et al., "Inducing the metal–support interaction and enhancing the ammonia synthesis activity of ceria-supported ruthenium catalyst via N2H4Reduction," *ACS Sustainable Chemistry & Engineering*, vol. 9, no. 13, pp. 4885–4893, 2021.

[26] J. Feng, L. Liu, X. Zhang et al., "Ru nanoparticles on Y_2O_3 with enhanced metal–support interactions for efficient ammonia synthesis," *Catalysis Science & Technology*, vol. 13, no. 3, pp. 844–853, 2023.

[27] B. Lin, B. Fang, Y. Wu et al., "Enhanced ammonia synthesis activity of ceria-supported ruthenium catalysts induced by CO activation," *ACS Catalysis*, vol. 11, no. 3, pp. 1331–1339, 2021.

[28] Y. Manaka, Y. Nagata, K. Kobayashi, D. Kobayashi, and T. Nanba, "The effect of a ruthenium precursor on the low-temperature ammonia synthesis activity over Ru/CeO_2," *Dalton Transactions*, vol. 49, no. 47, pp. 17143–17146, 2020.

[29] H. J. Park, A. Badakhsh, I. T. Im, M.-S. Kim, and C. W. Park, "Experimental study on the thermal and mechanical properties of MWCNT/polymer and Cu/polymer composites," *Applied Thermal Engineering*, vol. 107, pp. 907–917, 2016.

[30] A. Badakhsh and C. W. Park, "From morphology of attrited copper/MWCNT hybrid fillers to thermal and mechanical characteristics of their respective polymer-matrix composites: an analytical and experimental study," *Journal of Applied Polymer Science*, vol. 134, no. 41, p. 45397, 2017.

[31] T.-N. Ye, S.-W. Park, Y. Lu et al., "Contribution of nitrogen vacancies to ammonia synthesis over metal nitride catalysts," *Journal of the American Chemical Society*, vol. 142, no. 33, pp. 14374–14383, 2020.

[32] T.-N. Ye, S.-W. Park, Y. Lu et al., "Vacancy-enabled N_2 activation for ammonia synthesis on an Ni-loaded catalyst," *Nature*, vol. 583, no. 7816, pp. 391–395, 2020.

[33] X. Wang, X. Peng, W. Chen et al., "Insight into dynamic and steady-state active sites for nitrogen activation to ammonia by cobalt-based catalyst," *Nature Communications*, vol. 11, no. 1, p. 653, 2020.

[34] Y. Hu, G. Jiang, G. Xu, and X. Mu, "Hydrogenolysis of lignin model compounds into aromatics with bimetallic Ru-Ni supported onto nitrogen-doped activated carbon catalyst," *Molecular Catalysis*, vol. 445, pp. 316–326, 2018.

[35] F. Rouquerol, J. Rouquerol, K. S. W. Sing, P. Llewellyn, and G. Maurin, Eds., *Adsorption by Powders and Porous Solids*, Academic Press, Oxford, Second Edition edition, 2014.

[36] D. Klank and C. Reichenbach, "Particle World," Technical Papers of 3P Instruments, 2018.

[37] B. Lin, Y. Liu, L. Heng et al., "Morphology effect of ceria on the catalytic performances of Ru/CeO_2catalysts for ammonia synthesis," *Industrial & Engineering Chemistry Research*, vol. 57, no. 28, pp. 9127–9135, 2018.

[38] Y. Guo, S. Mei, K. Yuan et al., "Low-temperature CO_2methanation over CeO_2-supported Ru single atoms, nanoclusters, and nanoparticles competitively tuned by strong metal–support interactions and H-spillover effect," *ACS Catalysis*, vol. 8, no. 7, pp. 6203–6215, 2018.

[39] X. Wang, X. Peng, H. Ran et al., "Influence of Ru substitution on the properties of $LaCoO_3$ catalysts for ammonia synthesis: XAFS and XPS studies," *Industrial & Engineering Chemistry Research*, vol. 57, no. 51, pp. 17375–17383, 2018.

[40] J.-C. Liu, X.-L. Ma, Y. Li, Y.-G. Wang, H. Xiao, and J. Li, "Heterogeneous Fe_3 single-cluster catalyst for ammonia synthesis via an associative mechanism," *Nature Communications*, vol. 9, no. 1, p. 1610, 2018.